Available online at www.sciencedirect.com
SCIENCE DIRECT®
International Journal of Thermal Sciences 44 (2005) 219–233
International Journal of Thermal Sciences
www.elsevier.com/locate/ijts

Impact and solidification of indium droplets on a cold substrate

Cédric Le Bot *, Stéphane Vincent, Eric Arquis

Modélisation avancée des systèmes thermiques et écoulements réels (MASTER), ENSCPB, université Bordeaux 1, 16, avenue Pey-Berland, 33607 Pessac cedex, France

Received 15 July 2003; received in revised form 9 April 2004; accepted 13 July 2004

Available online 18 November 2004

Abstract

The present article reports on a numerical study of heat transfer and fluid flow characteristics during the impact and solidification of liquid droplets on a cold substrate. The impact dynamics and the associated thermal phenomena have been modelled by adopting a fixed grid (Eulerian) approach with a single set of mass, momentum and energy conservation equations. The VOF advection method with TVD front capturing approach has been utilized to track the time dependent droplets location and the interface between the solid, liquid and gas phases within the domain. Numerical experiments have been carried out for both simultaneous and sequential impact of indium liquid droplets on a cold substrate. Findings of the present study are deemed useful for better understanding and control of related surface coating and thin film manufacturing processes. The fluid behaviour and morphology of the resulting thin film have been found to be dependent upon the droplet impact velocity and frequency, and the fluid particles and substrate characteristics.

Keywords: Navier–Stokes; Droplet; Free surface; Numerical simulation; Surface tension; Solidification

1. Introduction

Modelling and simulation of heat transfer and fluid flow during the impact and solidification of liquid droplets on a cold solid substrate are useful tools for better understanding and control of related surface coating and thin film manufacturing processes.

For a single fluid droplet, numerous experimental [1,2] studies have been carried out at the droplet scale with or without solidification. Following the impact velocity and the droplet diameter, the fluid particle can adopt different forms of behaviour, from splashing to rebound and deposition. These different flows have been experimentally identified versus some parameters [3,4] such as impact velocity, droplet temperature, substrate temperature and materials chracteristics expressed by dimensionless numbers of Reynolds, Froude and Weber and the superheat parameter:

$$Re = \frac{\rho V_i D}{\mu}, \qquad Fr = \frac{V_i^2}{Dg}$$
$$We = \frac{\rho V_i^2 D}{\sigma}, \qquad \beta = \frac{T_{i,d} - T_f}{T_f - T_{i,\text{sub}}} \tag{1}$$

Solidification is also an influent behaviour upon the flow as the manner a droplet freezes alters the spreading velocity and the temperature field, as shown by Xu [5].

Some numerical works concerning a single droplet impact [6,7] have investigated these forms of behaviour by mobile or fixed mesh grids methods. They confirm the influence of Reynolds and Weber numbers on the kind of flow generated after impact thanks to the Sommerfeld number ($K = \sqrt{We\sqrt{Re}}$). The thermal exchanges and the solidification of the droplet are also taken into account to understand how they depend on flow dynamics. The pioneering works of Madejski [8] dealt with the study of the droplet spreading degree by numerical way after impact and its solidification taking two hypotheses into consideration: the solidification occurs once the spreading is finished, and the splat is considered as a disc with a constant thickness and a time–dependent diameter.

* Corresponding author. Tél.: +33 5 40 00 61 92, Fax: +33 5 40 00 66 68.
E-mail addresses: lebot@enscpb.fr (C. Le Bot), vincent@enscpb.fr (S. Vincent), arquis@enscpb.fr (E. Arquis).

1290-0729/$ – see front matter
doi:10.1016/j.ijthermalsci.2004.07.007

Nomenclature

a	thermal diffusivity	$m{\cdot}s^{-2}$
b	thermal diffusivity	$J{\cdot}m^{-2}{\cdot}K^{-1}{\cdot}s^{-0.5}$
C	phase function	
C_p	heat capacity	$J{\cdot}kg^{-1}{\cdot}K^{-1}$
D	droplet diameter	m
D_g	distance between two droplets	m
f	solid fraction	
$\mathbf{F_{ST}}$	source term of surface tension	N
$\mathbf{g}$	gravity	$m{\cdot}s^{-2}$
h	height	m
K_s	permeability	m^2
K	Sommerfeld number	
L_f	latent heat	$J{\cdot}kg^{-1}$
$\mathbf{n}$	interface normal	
P	pressure	Pa
Q	thermal energy	J
R	droplet radius	m
Re	Reynolds number	
S_c	source term of phase change	$W{\cdot}m^{-3}$
Ste	Stefan number	
t	time	s
T	temperature	K
TCR	thermal contact resistance	$K{\cdot}m{\cdot}W^{-1}$
$\mathbf{u}$	velocity	$m{\cdot}s^{-1}$
V_i	impact velocity	$m{\cdot}s^{-1}$
We	Weber number	

Greek symbols

β	superheat parameter	
δ	Dirac function	
Δx	infinitesimal thickness	m
κ	local curvature	m^{-1}
λ	thermal conductivity	$W{\cdot}m^{-1}{\cdot}K^{-1}$
μ	viscosity	Pa·s
ξ	solution of transcendantal equation	
ρ	density	$kg{\cdot}m^{-3}$
σ	surface tension coefficient	$N{\cdot}m^{-1}$

Indices

air	air
d	droplet
i	initial
ind	indium
int	interface
max	maximum
sol	solidification
sub	substrate

On the other hand, studies about multiple impacts are more rare. Many authors considered the solidification of the droplet by studying the influence of the substrate initial temperature on the morphology of a droplet colliding a previous solidified splat [9], the evolution of the solidification front when a droplet impacts a substrate of the same material [4] or the influence of the deposition of hot droplets on the previous one [10].

In the present work, we consider several metal droplets impacting sequentially onto a cold substrate in order to simulate the coating manufacturing. In the initial configuration (Fig. 1(a)), we consider several fluid particles colliding the substrate simultaneously and followed by some other droplets impacting on the previous fluid particles with a constant frequency. Two kinds of interactions can be observed: the meeting of two neighbouring droplets and the collision of a droplet onto the previous one. The first step consists in considering some droplets impacting at the same time onto the substrate without the next ones in order to analyze their behaviour during their meeting (that we call the meeting point) which originates from the formation of gas traps in thin film. These fluid particles are equidistant each other and D_g represents the distance between the center of two neighbouring droplets, as illustrated in Fig. 1(b). In the second step, we add to the previous step several identical droplets impacting one after the other along the same axis with a constant frequency (Fig. 1(b)) to take into account all the phenomena. By means of interactions between the neighbouring fluid particles and the following ones, we obtain a thin film whose porosity and surface heterogeneities are directly linked to the impact conditions in terms of velocities, particle diameter, distance between droplets and substrate and metal temperatures. Cartesian 2D configurations are first simulated (which means the impact of 2D cylinders) to lead a preliminary parametric study used to define clever 3D configurations, as these latter remain difficult to compute correctly. The aim of this choice is to give information about the dynamics and thermal behaviours, and about the occurrence of some surface heterogeneities (like air traps or surface topology) in order to use them in an actual coating manufacturing. From a qualitative point of view, dynamics and thermal phenomena are consistent with the expectations of 3D behaviour of the impact and the solidification of single particles. From a quantitative point of view, the two–dimensional character of heat and mass transfers enhances defaults like air traps and the heterogeneity of the surface of the thin layer. The appearance of these defaults convinced us of the interest of the parameters involved in the problem.

2. Numerical solution

In the present work, phenomena are described by the resolution of dynamics and thermal exchanges of a two phase flow, taking into account for solidification of one of these phases.

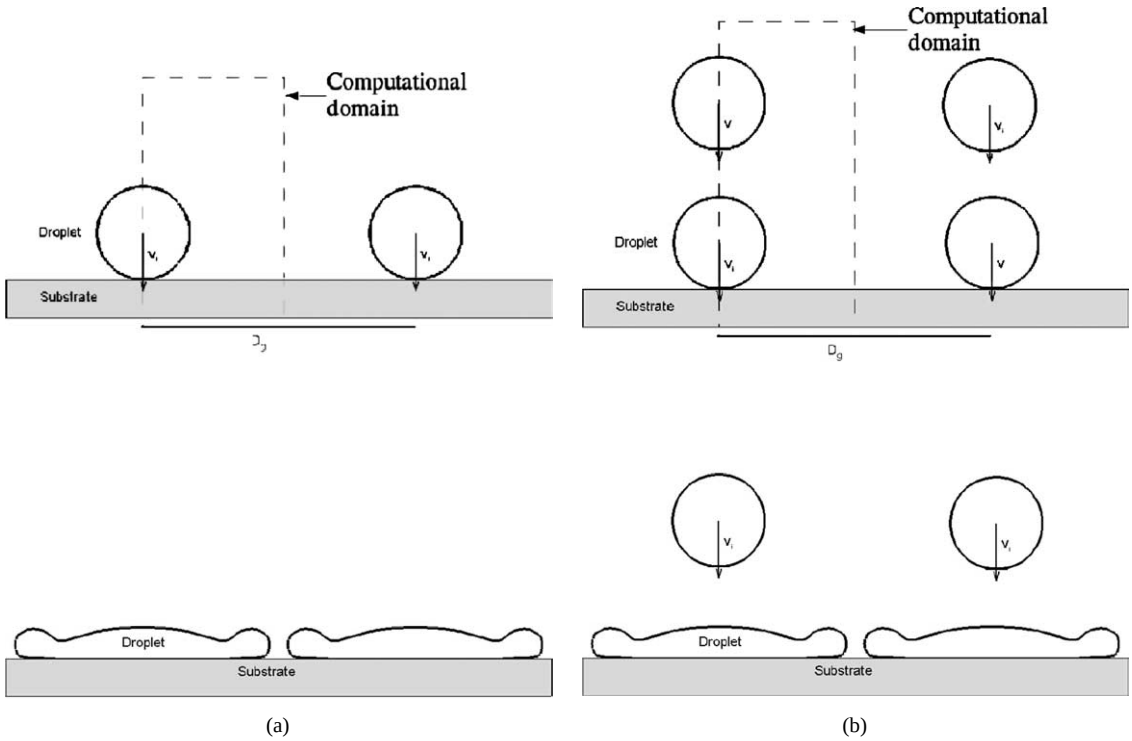

(a) (b)

Fig. 1. Actual and computational domains: (a) Simultaneous impact of droplets (b) Sequential impact of droplets.

2.1. Mathematical modelling

2.1.1. Flow dynamics

The droplet flow during the falling, the spreading and the meeting with neighbouring particles is modelled using momentum and continuity equations for incompressible flows in generalized formulation (in air, liquid indium and steel substrate):

$$\nabla \cdot \mathbf{u} = 0 \tag{2}$$

$$\rho\left(\frac{\partial \mathbf{u}}{\partial t} + \nabla \cdot (\mathbf{uu})\right) + \frac{\mu}{K_s}\mathbf{u} = -\nabla p + \rho \mathbf{g} + \nabla \cdot \mu\left(\nabla \mathbf{u} + \nabla \mathbf{u}^{\mathrm{T}}\right) + \mathbf{F_{ST}} \tag{3}$$

The term $\mathbf{F_{ST}}$ represents the force associated to the interfacial energy between air and droplet due to the surface tension and will be detailled later. The term $\frac{\mu}{K_s}\mathbf{u}$ or Brinkman term, allows to ensure zero velocity in regions where the permeability K_s is low (practically 10^{-20} m^2) to model a solid zone (substrate as well as solidified indium) using a penalty method [11].

2.1.2. Advection on the interface

To differentiate the solid, liquid and gas phases of the problem (air–droplet–substrate) we introduce a phase function C which corresponds to the fraction of each fluid in every control volume. The evolution of this variable is modelled by an advection equation:

$$\frac{\partial C}{\partial t} + \mathbf{u} \cdot \nabla C = 0 \tag{4}$$

This equation allows us to determine the droplets location according to the flow and to update their characteristics (density, viscosity, conductivity, specific heat) in every mesh, considering $C = 1$ when the mesh contains only droplet metal and $C = 0$ when it contains only air or substrate:

$$Var = C \cdot Var_d + (1 - C) \cdot Var_{\mathrm{air}} \tag{5}$$

where Var corresponds to the characteristics mentioned above.

The droplet–air interface is located where $0 < C < 1$ and is defined by $C = 0.5$. Moreover, the Navier–Stokes equations (3) and the advection equation (4) are coupled by taking into account the term F_{ST} in the momentum equation, which is calculated with the colour function C. This term is activated at the droplet–air interface, when $\|\nabla C\| \geqslant \varepsilon$ where ε is small. Some works show that this modelling approach provides a good accuracy (Brackbill [15]). It is calculated thanks to the knowledge of the interface location, with the local interface curvature κ, the unit norm at the interface n and the surface tension coefficient σ:

$$\mathbf{F_{ST}} = \sigma \kappa \mathbf{n} \delta \tag{6}$$

2.1.3. Thermal exchanges

Heat exchanges between droplet, air and substrate are modelled using the following energy equation:

$$\rho C_p\left(\frac{\partial T}{\partial t} + \mathbf{u} \cdot \nabla T\right) = \nabla(\lambda \nabla T) - S_c \tag{7}$$

The source term S_c corresponds to the occurrence of solidification and the possible remelting of the droplet. A thermal

contact resistance between the droplet and the substrate is introduced using a model based on a local modification of the thermal conductivity.

$$\lambda_{\text{eq}} = \frac{\Delta x}{\frac{\Delta x}{2\lambda_d} + TCR + \frac{\Delta x}{2\lambda_{\text{sub}}}} \tag{8}$$

The thermal contact resistance *TCR* is assumed to be a constant in our simulations.

2.2. Numerical methods

The equation system is described with a one fluid model using Cartesian coordinates on a staggered fixed grid (Eulerian approach). Eqs. (2) and (3) are discretized by a classical finite volume technique [12]. The numerical scheme is a second order scheme in time and space. The coupling between velocity and pressure is treated by an augmented Lagrangian algorithm [13,14] where the incompressibility constraint is satisfied by an iterative minimization algorithm.

The substrate and air are defined by the same color $C = 0$. Moreover, they are differentiated by permeability K_s which becomes very weak (with an arbitrary value of 10^{-20} m^2) into solid and thus ensures a zero velocity in this zone. In gas and liquid, it tends to infinity (practically $K_s = 10^{40}$ m^2).

The resolution method for C used in this work is based on a front capturing approach called Lax Wendroff TVD (Total Variation Diminishing) [16] that consists in rebuilding the solution for the colour function C assuming linear variation of the solution in each cell. Even if it induces small numerical diffusion on two or three mesh cells, the advantage of this method compared to a geometric VOF–PLIC method [17] is to be less sensitive to high frequency interface perturbations and then to more effectively evaluate the influence of the surface tension.

The competition of surface energies between the substrate, the droplet and air leads to the presence of a contact angle θ between these media. Numerous authors studied this phenomenon and determined some values of θ based on experiments. Jamet et al. [18] introduce these data in the numerical resolution through a boundary condition for the colour function:

$$(\nabla C \cdot \mathbf{n_s})_{\text{wall}} = \|\nabla C\| \cdot \cos(\theta) \tag{9}$$

Because of nonlinearity and hysteresis behaviours, modelling the contact angle remains a difficult problem for continuum models.

The energy equation is solved by a hybrid centered—UPWIND scheme [12]. The source term $S_c = \rho L_f \frac{\partial f}{\partial t}$ and the associated solid fraction f are taken into account numerically by a fixed point algorithm on the energy equation based on the "New Source" method [19], assuming that the behaviour law of the source term is linear with respect to temperature [20]. The nodes where the phase change occurs are maintained at the phase change temperature until solidification is completed.

The Navier Stokes and energy equations are linked by a solid fraction law versus permeability (penalty method). Once the solidification is fully achieved on the concerned node, i.e., the solid fraction is equal to 1, a very weak value of permeability is imposed to block velocities (cf previous part). Conversely, if at the concerned node remelting takes place, a large value is attributed to the permeability.

3. Results and discussion

In the present work, the study is limited to the cases where the Weber and Reynolds numbers allow the droplets to be deposited onto the substrate while avoiding instabilities due to the splashing phenomenon. We consider wide ranges of Reynolds and Weber numbers respectively of $108 < Re < 10814$ and $0.46 < We < 46$.

A study on the meshgrid influence shows that the spreading degree and the dimensionless height of a single droplet are consistent with mesh independence for a range of 40×40 to 100×100 meshgrids (Fig. 2).

3.1. Validation and comparisons

The study of the impact of a single droplet has been carried out by numerous authors. The numerical code described in this paper was used by Vincent et al. [21] to investigate the behaviour of one droplet impacting onto a solid surface. To check our results, a preliminary study is carried out on the deposition of a water droplet, in order to compare the results to an experiment [22] and a numerical solution proposed by Francois and Shyy [23,24]. One

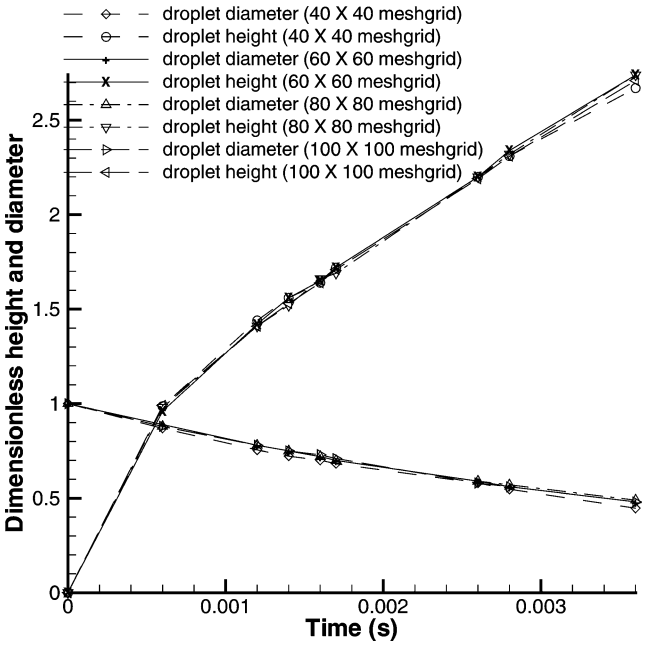

Fig. 2. Variation of dimensionless height and diameter with time during water droplet impact using different grid sizes ($Re = 3200$ and $We = 30$).

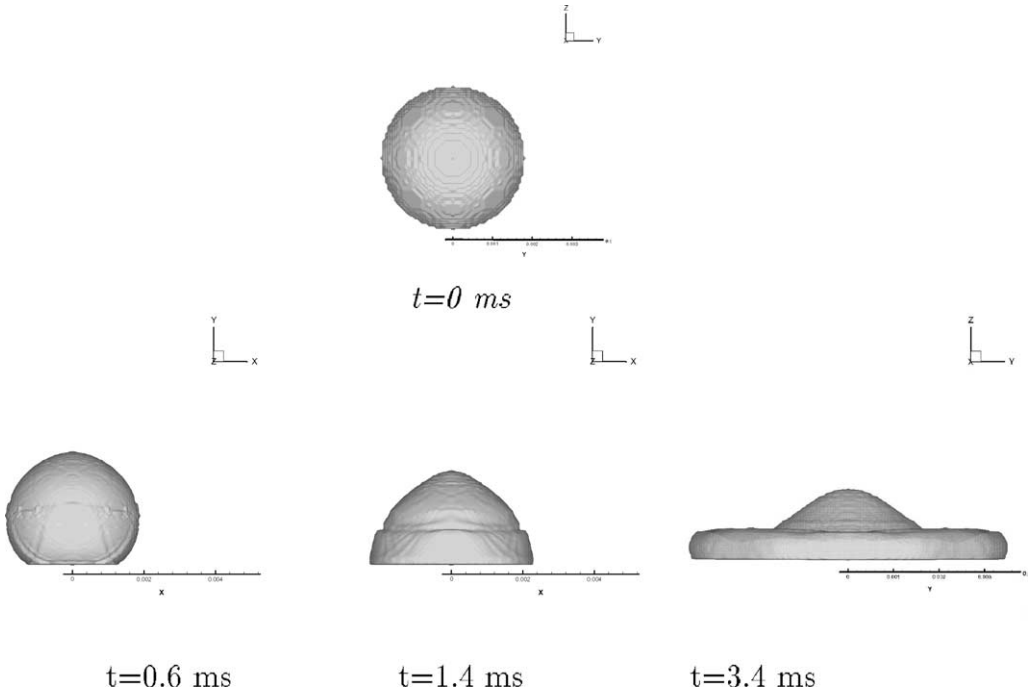

Fig. 3. Numerical simulation of a water droplet, to compare with data of Francois et al. [23].

consider a water droplet with the following impact parameters: $D_i = 3.6$ mm, $V_i = 0.77\ \mathrm{m{\cdot}s^{-1}}$, $\rho_{\mathrm{water}} = 996\ \mathrm{kg{\cdot}m^{-3}}$, $\mu_{\mathrm{water}} = 8.67 \times 10^{-4}$ Pa·s and $\sigma_{\mathrm{water}} = 0.0717\ \mathrm{N{\cdot}m^{-1}}$. It corresponds to dimensionless Reynolds and Weber numbers of $Re = 3200$ and $We = 30$. The 3D numerical domain is 3.6×10^{-3} m width and 4.8×10^{-3} m high and the meshgrid corresponds to a regular $60 \times 60 \times 80$ nodes mesh. One of the difficulties of such a problem concerns the contact angle between the substrate and the droplet. This parameter influences the spreading and recoil phenomena and remains hard to compute correctly. Several investigations were carried out to input values of contact angle from experimental data [25] and results show that a dynamic contact angle must be used. Our calculations do not contain any explicit model concerning contact angle because of the nature of the one fluid model. Nevertheless, results exhibit a good agreement with the experimental and numerical data supplied by Francois et al. [23] as it is shown on Fig. 3. The main difficulty encountered in this simulation consists in a long computation time due to a high number of nodes necessary to obtain an accurate result. That is why a 2D simulation is leaded in order to examine the dynamics and thermal phenomena qualitatively speaking with quite rapid results.

3.2. Simultaneous impact of droplets

The numerical configuration used for this 2D simulation corresponds to half of one droplet following a symmetry plan assumption (Fig. 1). Boundary conditions are the following: on the left and right sides, symmetry is considered for velocity and adiabatic for heat transfer. At the bottom, a wall condition is imposed (velocity equal to zero) for velocity and a constant temperature ($T = 25\,^{\circ}\mathrm{C}$) is chosen whereas at the top, there is a Neumann condition for velocity and an adiabatic one for heat transfer. This configuration allows to simulate the simultaneous impact of an infinity of identical droplets equidistant at D_g. This is a way to study interactions between close fluid particles through the height of two meeting droplets. In this study, ranges of Reynolds and Weber numbers are chosen ($108 < Re < 1081$ and $0.46 < We < 46$) in order to ensure a splat phenomenon, i.e., deposition without secondary droplets.

3.2.1. Flow dynamics

The time evolution of droplets shape is illustrated on Fig. 4 where $Re = 1081$ and $We = 29$. The 2D droplet spreads onto the substrate with a morphology that could be compared to a peripheral crown in a 3D case. This behaviour was found in previous 2D and 3D studies [26,27] concerning impact of an insulated droplet onto a substrate. Then, the droplet reaches the symmetry plan where it meets another droplet. This meeting implies a jet of matter towards the top: the spreading kinetic energy is partially converted into surface energy, viscous forces and solidification works. The part of energy that is still not dissipated is converted into kinetic energy inducing a jet of matter. This jet reaches a maximal value called $h_{\max}$. This energy, which corresponds to a part of the initial kinetic energy, generates a rising lower than the initial droplet height and is counteracted by the surface tension. This rising of matter goes back down and comes back towards the droplet impact, generating a back wave. Kinetic energy is dissipated again by viscous forces work and superficial energy. These oscillations of matter continue until there is total dissipation of energy and thus stabilisation of

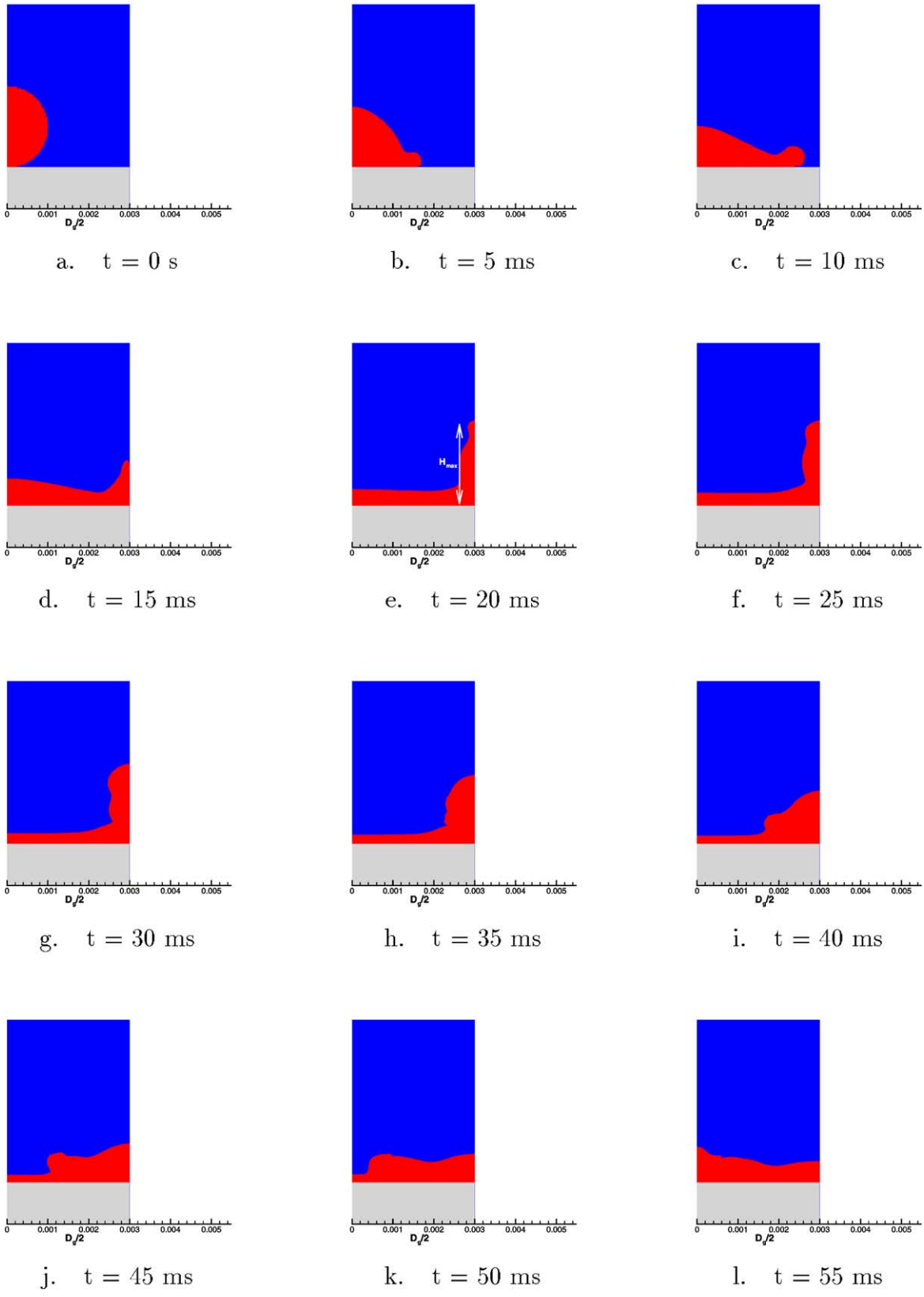

Fig. 4. Example of droplets impact simulation with $V_i = 0.1$ m·s^{-1} and $D_i = 2$ mm ($Re = 1081$ and $We = 29$).

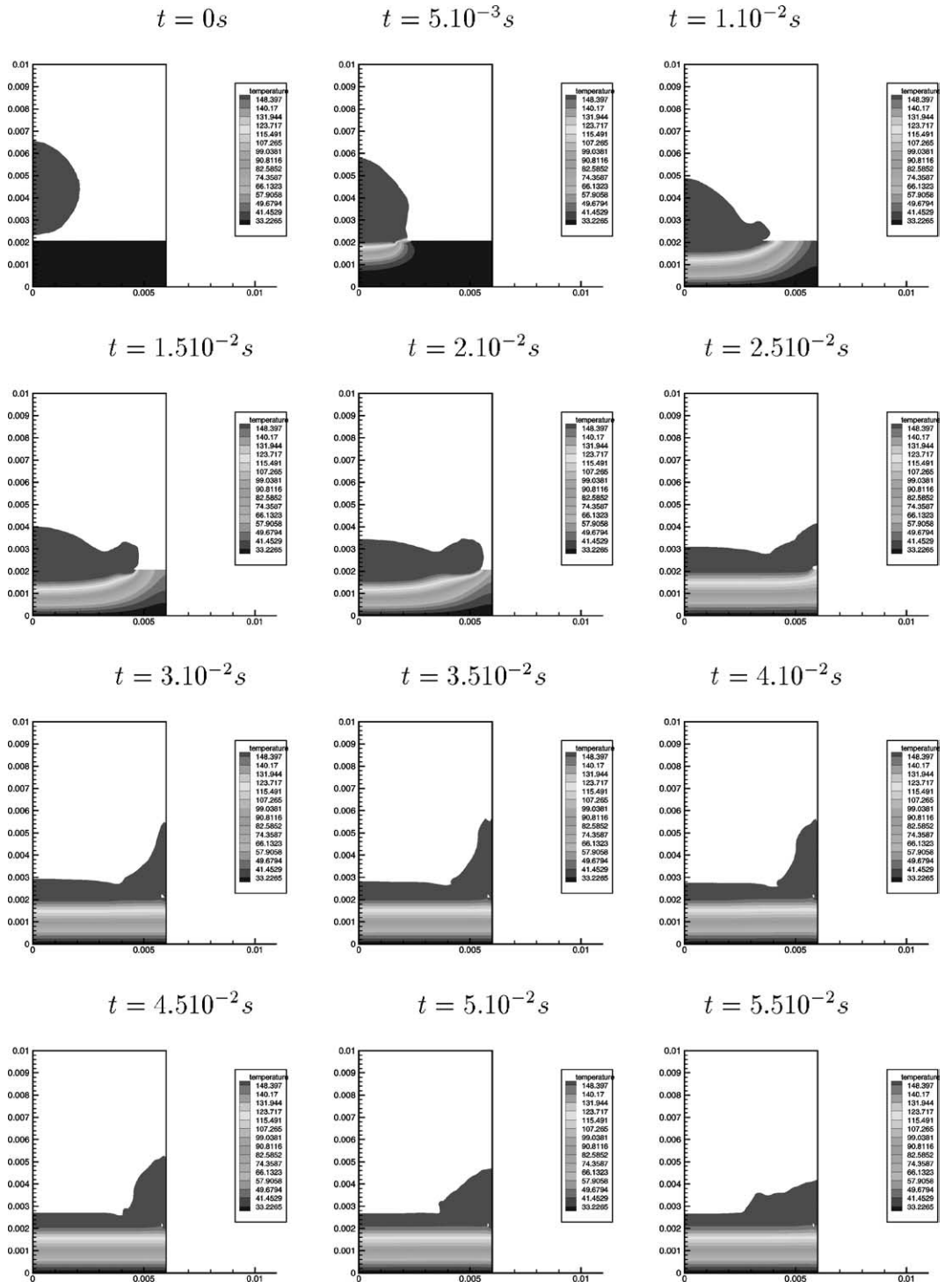

Fig. 5. Thermal field of simultaneous impact. Time step: $\Delta t = 10^{-5}$ s, mesh $60 * 100$ with $D_g = 6$ mm and $H = 10$ mm. Initial impact velocity: $V_i = 0.2$ m·s^{-1}, initial droplet size: $D = 4$ mm ($Re = 2162$, $We = 0.53$ and $Ste = 0.3$).

the thin film (Fig. 5). The heights of the droplet at impact and of the jet of matter at the meeting of two droplets, depend on several parameters: the droplet impact velocity , the surface tension, the solidification rate and the distance between the droplets.

In order to study these dimensionless numbers independantly, we have chosen to vary the metal viscosity to examine the effect of the Reynolds number on the maximum meeting height which is reached when two droplets meet each other the first time. Then only the surface tension is altered to see the influence of the Weber number upon the maximum meeting height. The influence of these parameters can be interpreted in the same way: when the droplet viscosity or the surface tension increases, the conversion of

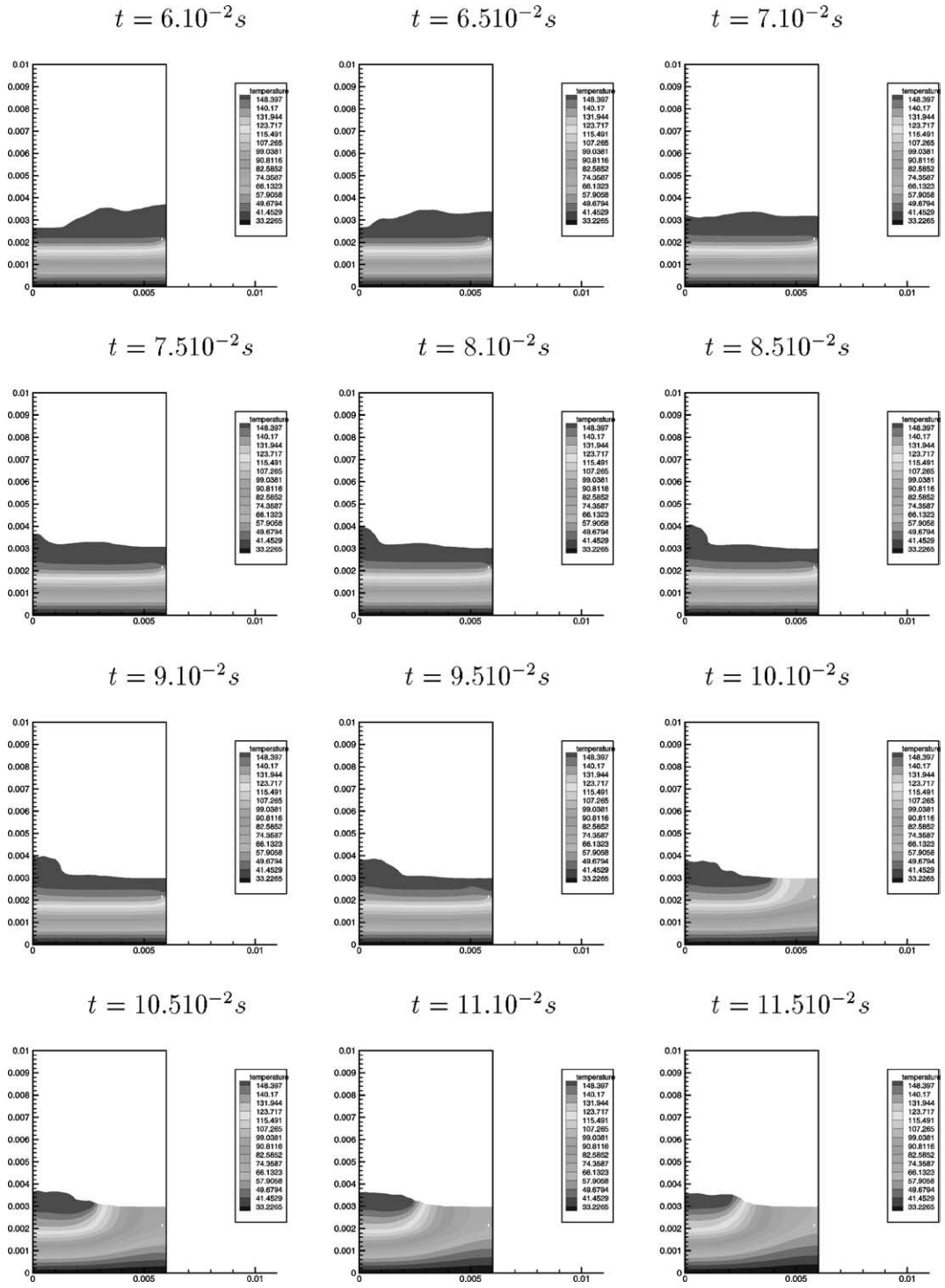

Fig. 5. (Continued).

the initial kinetic energy (due to the initial impact velocity) into viscous forces work (of surface energy) is greater. Thus when two droplets meet each other, the kinetic energy available is less important and the resulting meeting jet is less high. This is represented on Figs. 6 and 7 where the meeting jet rises with the Reynolds number or the Weber number. The results show that for $Re = 108$, the dimensionless maximum meeting height reaches a value of 1.15 and for $Re = 1081$, we obtain $h_{\max}/D_i = 1.35$. In this range of Reynolds numbers, the results exhibit a linear behaviour of the dimensionless height versus $\mathrm{Ln}(Re)$:

$$\frac{h_{\max}}{D_i} = 0.09\ln(Re) + 0.727 \tag{10}$$

With a constant Reynolds number and different Weber numbers, results are closed to a linear behaviour of the dimensionless meeting height versus Ln(*We*), from $We = 14.6$ where $h_{\max}/D_i = 0.78$ to $We = 146$ for which $h_{\max}/D_i = 1.40$:

$$\frac{h_{\max}}{D_i} = 0.27\ln(We) + 0.12 \tag{11}$$

The range of Weber numbers is limited because of an high surface tension value (low Weber number) which results in rapid recoil so that droplets cannot meet the neighbouring ones, and a low surface tension value (high Weber number) which corresponds to the limit before splashing phenomenon.

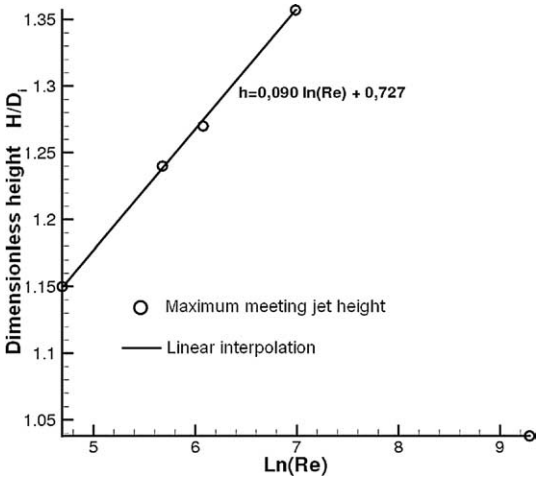

Fig. 6. Droplet meeting height versus the Reynolds number.

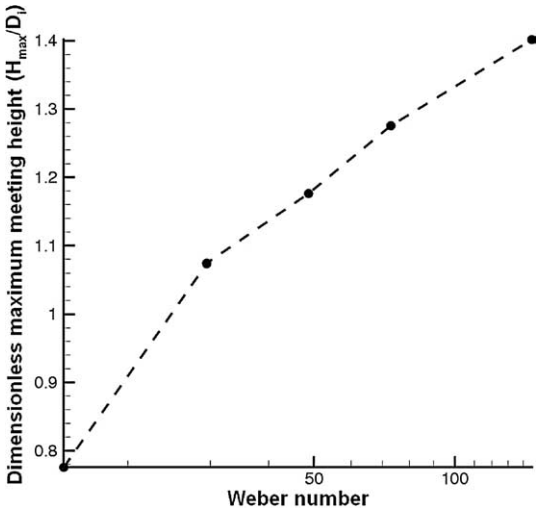

Fig. 7. Droplet meeting height versus the Weber number.

The droplet solidification at the substrate contact during the spreading alters the spreading behaviour, as with the solidification of the peripheral zone, the matter still in flow meets an obstacle and it creates a splash of small amplitude. The droplet continues spreading but an air trap, with small dimensions, is created at the substrate surface at the meeting location of two droplets. This zone where the phase function is equal to zero widens on several meshes, and seems to keep about the same area whatever the meshgrid is. This air trap is emphazised by the bidimensional character of the domain. For a stronger impact velocity ($V_i = 0.2\ \mathrm{m\cdot s^{-1}}$), convection delays solidification and the meeting of droplets occurs without any perturbation caused by phase change. The air trap is then smaller than in the case of $V_i = 0.05\ \mathrm{m\cdot s^{-1}}$.

3.2.2. Thermal exchanges and solidification

In order to evaluate the evolution of thermal exchanges during spreading, the surface substrate temperature at the impact and the meeting positions, and the heat flux density at the same positions are picked up (Fig. 8). The indium droplet is initially hot with an homogeneous temperature of $T_{\mathrm{ind},i} = 190\,^{\circ}\mathrm{C}$ and the steel substrate is cold with a temperature of $T_{\mathrm{sub},i} = 100\,^{\circ}\mathrm{C}$. Physical characteristics are reported in Table 1. Heat transfer begins as of the contact between the cold substrate and the hot droplet. Fig. 5 exhibits qualitatively thermal exchanges between simultaneous droplet impacts and the cold substrate. At the impact position, the contact temperature increases rapidly to reach a maximum value of $T = 166\,^{\circ}\mathrm{C}$ (Fig. 12). Then it decreases slowly during the droplet spreading as the substrate is not maintained at a constant temperature. This result can be compared to the analytical interface temperature of two media suddenly in contact without thermal contact resistance one undergoing solidification, following expressions [28]:

$$T^* = \frac{T_f b_{\mathrm{ind}} + T_{\mathrm{sub},i} b_{\mathrm{sub}}\,\mathrm{erf}(\xi)}{b_{\mathrm{ind}} + b_{\mathrm{sub}}\,\mathrm{erf}(\xi)} \tag{12}$$

with T^* the interface temperature considered as constant and ξ the solution of the transcendantal equation:

$$\frac{\exp(-\xi^2)}{\mathrm{erf}(\xi)} + \frac{\lambda_{\mathrm{ind,liq}}}{\lambda_{\mathrm{ind,sol}}}\sqrt{\frac{a_{\mathrm{ind,liq}}}{a_{\mathrm{ind,sol}}}} \times \frac{T_f - T_{\mathrm{sub},i}}{T_f - T^*}\frac{\exp(-\xi^2\frac{a_{\mathrm{ind,sol}}}{a_{\mathrm{ind,liq}}})}{\mathrm{erfc}(\xi\sqrt{\frac{a_{\mathrm{ind,sol}}}{a_{\mathrm{ind,liq}}}})} = \frac{\xi L_f\sqrt{\pi}}{Cp_{\mathrm{ind}}(T_f - T^*)} \tag{13}$$

Table 1
Physical properties of materials

Material	Density [kg·m^{-3}]	Conductivity [W·m^{-1}·K^{-1}]	Specific heat [J·kg^{-1}·K^{-1}]	Viscosity [Pa·s]	Latent heat [J·kg^{-1}]
Indium	7300	81.2	233	1.35×10^{-3}	28.6×10^{3}
Substrate	7350	36.5	465	–	–
Air	1.17	0.268	1006	1.85×10^{-5}	–

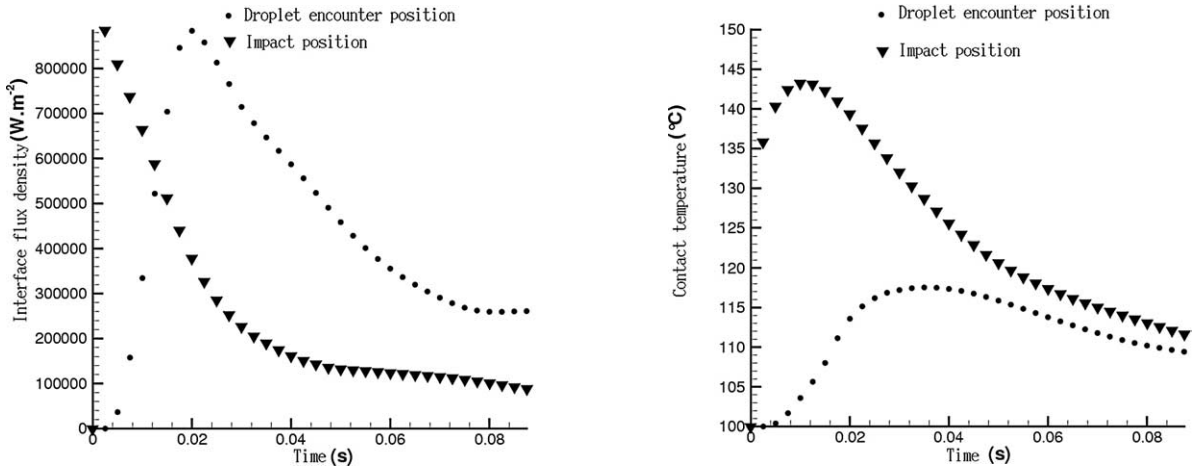

Fig. 8. Flux density and contact temperature at the substrate surface at impact and meeting positions ($Re = 1081$, $We = 14.6$, $D_g = 6$ mm, $T_{\text{sub},i} = 100\,^{\circ}\text{C}$ and $T_{\text{ind},i} = 190\,^{\circ}\text{C}$).

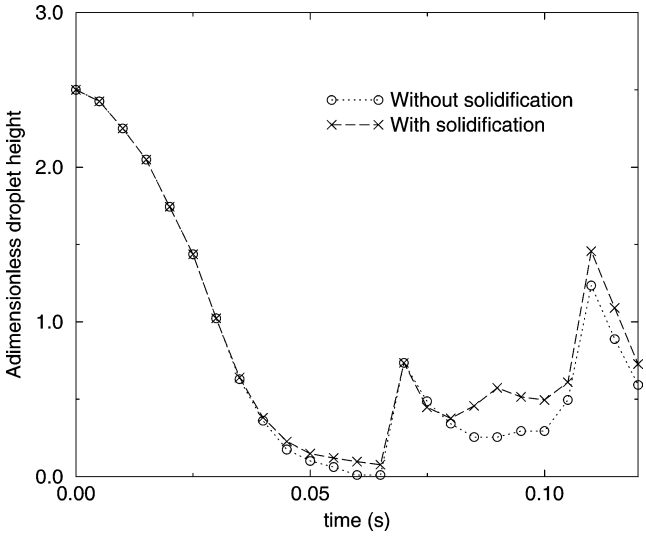

Fig. 9. Droplet heights at the impact location with and without solidification.

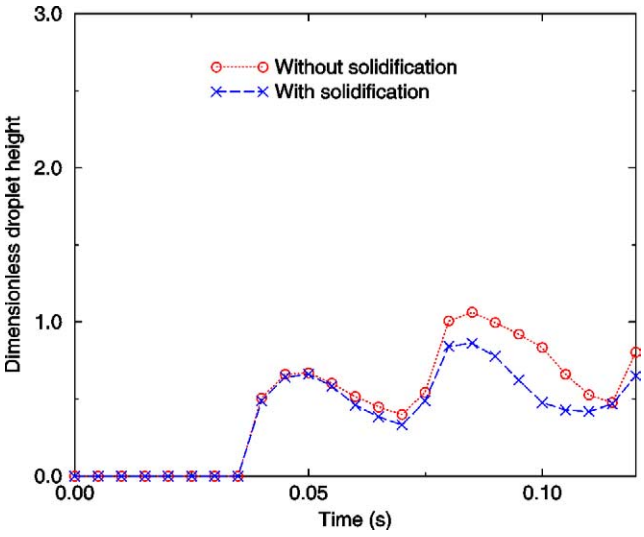

Fig. 10. Droplet heights at the meeting location with and without solidification. $Re = 1081$, $We = 1.3$, $Ste = 0.3$.

The analytical temperature computed with these expressions is evaluated to $T_{x_1,\text{tcr}=0} = 152\,^{\circ}\text{C}$. The numerical value obtained is greater than the analytical one. That can be explained by the following way: the droplet flow plays an important role in thermal exchanges. The flow locally brings heat by convection to the substrate during the first steps of the spreading whereas the theoretical expression assumes that only conduction takes place. Moreover, this analytical formula does not take into account the thermal contact resistance which is imposed to a value of $RTC = 10^{-5}\ \text{K}\cdot\text{m}^2\cdot\text{W}^{-1}$ in our simulations.

As the liquid spreads, its thickness becomes weak and the droplet ceases to supply heat to the substrate. Then the interface temperature at the substrate side decreases slowly during the droplet solidification until 0.02 s at the impact position and until 0.03 s at the meeting position (Fig. 12). When the entire metal is solidified, the interface temperature decreases more rapidly as the latent heat is totally released (from 150 to 130 °C at the impact position and from 145 to 130 °C at the meeting position). The solidification rate is directly linked with the initial substrate and droplet temperatures. Some experiments [9] show that an initially hot substrate implies a disc-shaped splat whereas a cold substrate generates star-shaped splashes. This kind of phenomenon can be examined through the Stefan number defined as:

$$Ste = \frac{C_P \Delta T}{L_f} \tag{14}$$

where ΔT is the difference between the initial substrate temperature (called $T_{\text{sub},i}$) and the phase change one (T_f). The effect of solidification on the flow can be underlined by studying the droplet height at impact and meeting positions against the Stefan number. This latter parameter is altered by modifying the substrate initial temperature. Results show that when $T_{\text{sub},i} = 50\,^{\circ}\text{C}$ (corresponding to $Ste = 0.87$), the dimensionless meeting point height reaches a maxi-

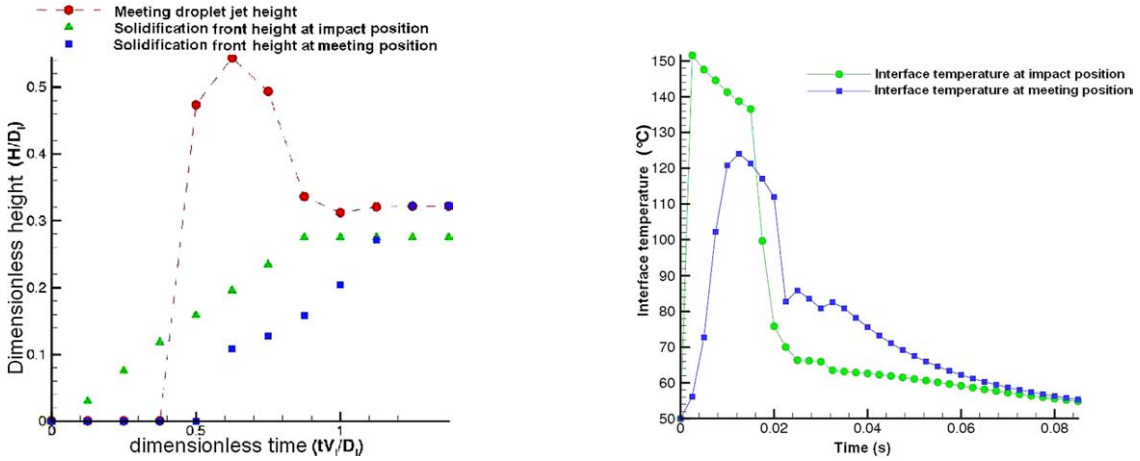

Fig. 11. Dimensionless droplet height and solidification front height at impact and meeting locations and contact temperatures at the same positions ($Re = 1081$, $We = 15$, $D_g/D_i = 3$ and $Ste = 0.87$).

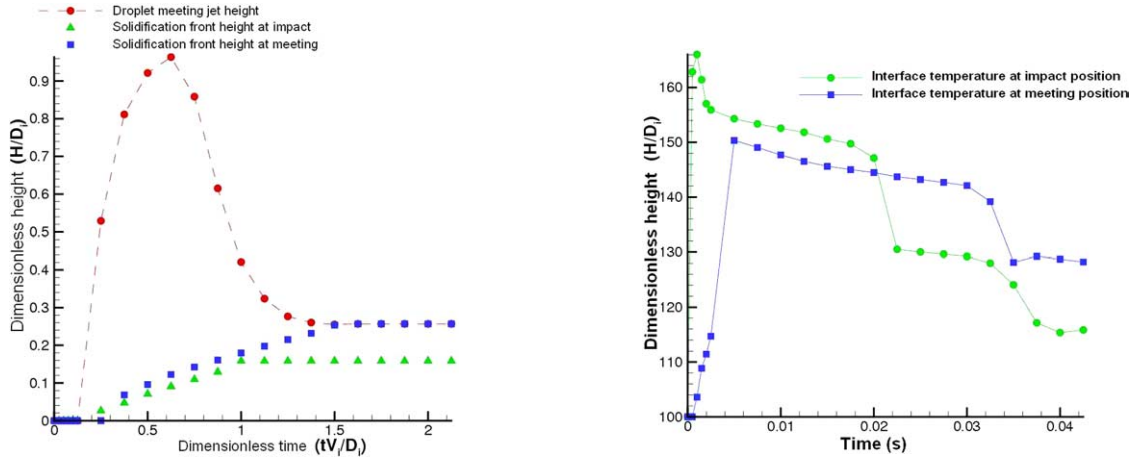

Fig. 12. Dimensionless droplet height and solidification front height at impact and meeting locations and contact temperatures at the same positions ($Re = 1081$, $We = 15$, $D_g/D_i = 3$ and $Ste = 0.46$).

mum value of $h_{e,\max} = 0.54$ whereas $T_{\text{sub},i} = 100\,^{\circ}\text{C}$ (i.e. $Ste = 0.46$) provides $h_{e,\max} = 0.96$. Initialising a low substrate temperature means that the initial kinetic energy is more converted into work necessary to freeze the fluid. As less kinetic energy is available at the droplet meeting in such a case, it results in a small meeting droplet jet. Solidification also decreases the time required to stabilize the thin film by blocking the matter (Figs. 9 and 10). Without solidification, matter flows more and then the thin film thickness at the impact location reaches a smaller value. On the other hand, at the location of the meeting of two drops, the kinetic energy is more significant when the phase change is not active, since there is no conversion of this energy into solidification work. Consequently, the jet produced upon the meeting of two droplets is higher when solidification does not occur. This situation implies that the fluid oscillations around the steady state thickness last longer when there is no phase change. Thus, the final coating is consequently manufactured rapidly but it implies that the surface topology is not flat, as it can be seen of Figs. 11 and 12 where the droplet heights at the impact and the meeting positions are not the same.

As it can be seen on Fig. 13, the solidified droplet heightens at the impact axis and the droplet meeting axis evolves identically. Thus, we observe from our 2D simulations that the solidification exhibits a 1D behaviour during the spreading and meeting of two particles. The competition between the time necessary to freeze the droplets and the time necessary to convert the kinetic energy in the others energies (viscous forces ...) can lead to different final coatings: if the solidification rate is important enough, the fluid is totally frozen before the equilibrium thickness e_{eq} along all the substrate is reached. It results in a nonuniform coating relief, which means that the solidification time value can imply a smooth or a rough surface topology.

3.3. Sequential impact of droplets

3.3.1. Flow dynamics

In order to study numerically the coating manufacturing, interactions between impacting droplets and the pre-

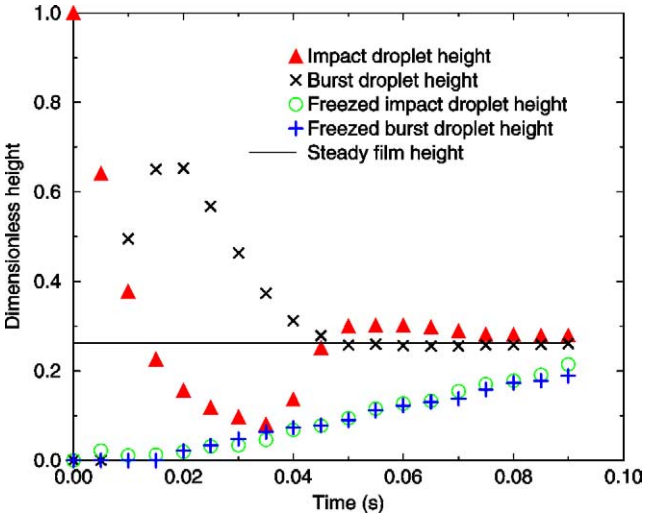

Fig. 13. Dimensionless droplet height and solidification front height at impact and meeting locations ($Re = 1081$, $We = 1.3$, $Ste = 0.3$).

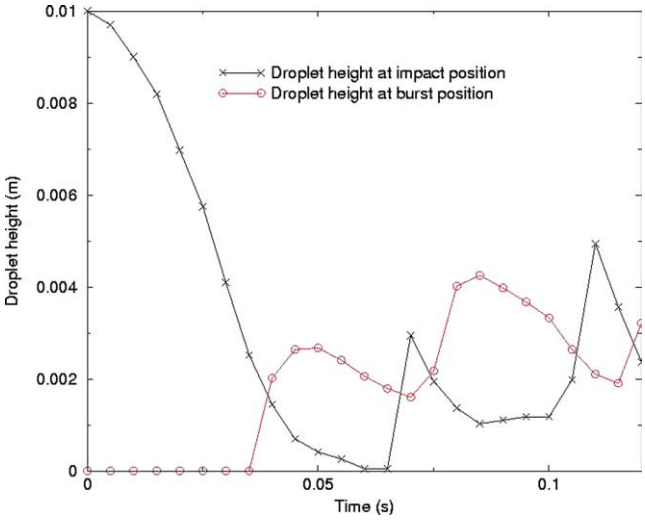

Fig. 14. Substrate heights during the impact of successive droplets. $Re = 1081$, $We = 1.3$.

vious splat (totally solidified or not) have to be simulated. Some studies have been carried out about droplets pileup [29] where the fluid particles impact onto a previously solidified droplet. The configuration of our case is the impact of simultaneous and successive droplets onto the substrate with a constant frequency. The boundary conditions of the previous case are conserved in order to simulate the impact of droplets from a spray coating. The impact frequency, f, is an additional parameter which can determine the film morphology. Effectively, it defines kinetic energy and heat amounts brought to the system by regular time intervals. When the frequency is high, the impact kinetic energy is added, whereas the rising of the meeting jet of two droplets is not finished. It accumulates and therefore it amplifies the jet height (Fig. 14). For droplets impacting onto the substrate with $Re = 1081$ and $We = 1.3$ and a frequency $f = 2.5\ \mathrm{s}^{-1}$, one observes that the droplet impact and meeting heights in-

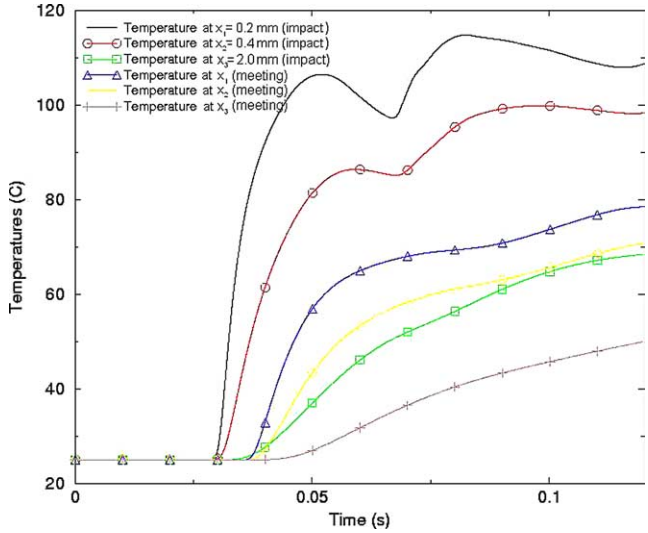

Fig. 15. Substrate temperatures during the impact of successive droplets. $Re = 1081$, $We = 1.3$.

crease recurringly, and this recurrence corresponds to the impact frequency. As fluid is progressively added, the first maximum meeting height reaches a dimensionless value of 0.62 and the second one is about 1.1. Even if the rising jet becomes higher and higher while droplets successively impact, this rising is less and less significant if we compare it to the film thickness. Effectively, the behaviour evolves, from impact onto a dry substrate to impact onto a liquid film or a solidifying one. During the first impact, the droplet spreads along the solid substrate and kinetic energy is converted into surface energy and viscous forces work. When the second droplet impacts onto the previous one, it comes in contact with a moving liquid surface. Its kinetic energy is converted into the other kinds of energies and works but it is also transmitted in the liquid layer, which diminishes the kinetic energy amount available at the meeting position. It results in a second droplet meeting height smaller than the previous one. Thus during the successive impacts, there is less and less kinetic energy brought to the meeting location and consequently the altitude of the jet of metal is not as high.

3.3.2. Thermal field and solidification

During the sequential impact of droplets, thermal phenomena described in the previous part (simultaneous impacts) also occur during the first moments, as it corresponds to that case during this time. When next droplets come in contact with the first one, the thermal field is rapidly perturbated (Fig. 15) under the impact location and the location where two droplets meet each other. The Fig. 15 illustrates temperatures picked up in the substrate, under impact and meeting positions at different depths x_1, x_2 and x_3. The substrate is initially held to $T = 25\,^{\circ}\mathrm{C}$ and the droplet is hot at $T = 190\,^{\circ}\mathrm{C}$. At the impact of the first droplet, the substrate temperatures under the impact position increase from $T = 25\,^{\circ}\mathrm{C}$ to different values following the depth: $107\,^{\circ}\mathrm{C}$ at

$x_1 = 0.2$ mm from the substrate surface and 87 °C at $x_2 = 0.4$ mm. The temperature at $x_3 = 1$ mm increases gradually as the temperature variation due to the sequential impact of hot droplets is less marked at this depth than x_1 and x_2. Temperatures begin to decrease because thermal diffusion takes place in the substrate and as the droplet spreads, it does not supply thermal energy to the substrate. When the second droplet impacts onto the previous one, it supplies heat again to the substrate and substrate temperatures rise again with maxima values of $T = 118\,°C$ at x_1 and $T = 99\,°C$ at x_2. For the temperature at x_3, one observes that it still increases as it is deep enough to undergo a progressive heating. A short delay is observed for temperatures under the meeting position which corresponds to the time necessary for liquid to reach the meeting position. Then the same behaviour than at the impact position is observed but with lower temperatures as indium is cooled during impact and spreading. With a long enough time and considering our thermal boundary conditions (adiabatic), the supply will prevent the solidification, which is why the simulation is halted before boundary conditions alter behaviour. Nevertheless, thermal exchanges between the droplets and the substrate are more important during the first impact than during the following ones. These exchanges are attenuated by a weaker temperature difference between the droplet and the new impact surface either solid (if droplets are already solidified) or liquid (particles still liquid), than by the differences between the drop and the substrate and by the thermal properties of the surface. It means that the supply of thermal energy by the next droplets has little influence upon the thermal variation of the substrate. It also implies that the solidification rate slows down and therefore that the thermal phenomena controling solidification are preponderant only during the impact of some successive layers, the next ones having no effect on it.

Solidification alters the droplet dynamics as from the contact with the cold substrate. Comparing the droplet heights at the impact location and the meeting location (Fig. 16), in the cases with and without phase change, it can be noticed that solidification causes a larger metal thickness at the impact location during the entire simulation time. On the contrary, at the meeting location, solidification diminishes the height of the meeting jet. A part of the kinetic energy is converted into the energy required for the solidification process, that blocks the metal and decreases the reaction of the meeting jet. Thus, while solidification occurs, the droplet flow rapidly slows down between the impact location and the meeting one and consequently the jet becomes smaller. The droplet metal is blocked and the thin film reaches a steady state more rapidly. On the other hand, the coating relief becomes heterogeneous as the film is frozen before it reaches a state of equilibrium.

Fig. 17 shows the droplet heights at the impact location and the meeting location and the solidified thicknesses. As explained previously, the metal heights at the two locations increase progressively during every impact. On the other hand, the solidification front is altered by the second impact(at $t = 0.07$ s) but not by the third one at $t = 0.11$ s (Fig. 16). At $t = 0.07$ s, there is a partial remelting of metal at the impact location directly at the time of the impact of the next droplet. The thickness of the first layer at $t = 0.07$ s at the impact location is feeble enough to allow the heat supply to remelt the layer. The heat amount to bring to the layer in order to remelt metal for a thickness of δx_{sol} and along a surface area equal to $\Delta y \cdot 1$ is $Q_{\text{sol}} = \rho L_f \delta x_{\text{sol}} \Delta y$. But the new droplet has initial thermal energy $Q_d = \rho C_p T_d (\pi D_g^2/4)$. Considering that the remelted layer area is $\Delta y \cdot 1 = 1.10^{-4}\,\text{m}^2$, the energy ratio necessary to partially remelt the metal in the present case (indium droplets initially at $T_{\text{ind},i} = 190\,°C$) is equal to 0.5%, the rest of the energy being transmitted into the still liquid layer by diffusion and convection. Then, solidification increases again, as the new droplet cools down. At $t = 0.11$ s, the new layer

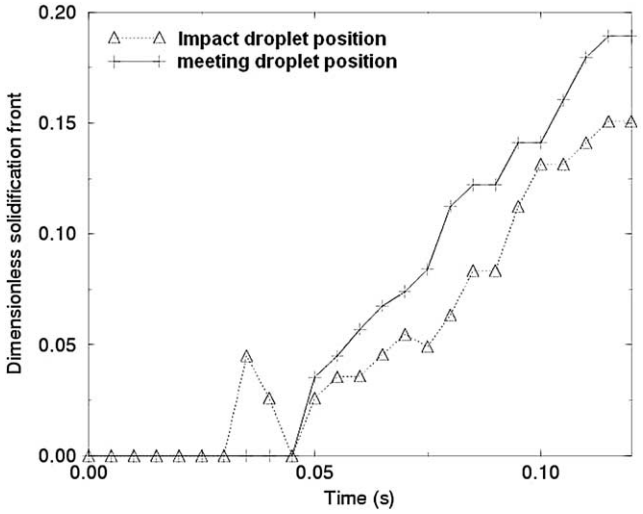

Fig. 16. Dimensionless solidified metal heights. At $t = 0.07$ s and $t = 0.11$ s, impact of new droplets. $Re = 1081$, $We = 1.3$, $Ste = 0.3$.

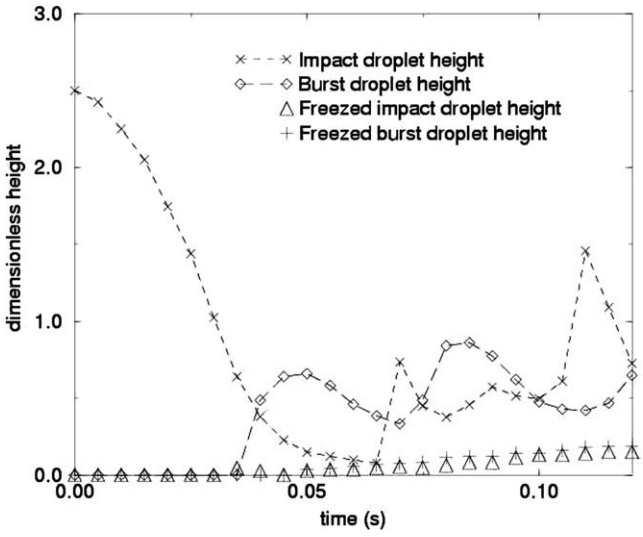

Fig. 17. Droplet heights at the impact and meeting locations and solidifyed droplet heights. $Re = 1081$, $We = 1.3$, $Ste = 0.3$.

thickness is greater than the one at $t = 0.07$ s. At the impact location, the new layer cannot supply enough heat to initiate remelting. However it disrupts it by slowing its progression. Thus, at the third series of impacting droplets, the solidification front is not altered by heat supply from the next fluid particles.

4. Conclusion

This numerical study is carried out to characterize parameters influencing the morphology of a thin film created by spraying metal droplets onto a substrate. In the case of the simultaneous impact of droplets, the stabilisation of the thin film depends on the impact velocity of the fluid particle, on the distance between two neighbouring particles and on the metal solidification rate. The kinetic energy of each droplet is converted into surface energy and solidification and viscous works. Depending on the impact velocity, the stabilisation of the layer can be more or less rapid and liquid oscillations are generated and dissipated by conversion of the kinetic energy. The time necessary to stabilize the thin film depends on the surface tension, the metal inertia and the solidification rate. This last parameter speeds up the transformation of the kinetic energy and influences the relief of the film, since rapid solidification can freeze matter before the equilibrium thickness is reached along the substrate.

At the meeting of two droplets, the peripheral crown of each one contributes to the creation of an air trap at the substrate surface. The metal solidification around this trap blocks the air, which implies a heterogeneous thermal contact along the substrate and more difficult heat transfer in the zones where droplets meet each other. Thus, couplings between thermal and dynamic behaviours define the porosity and the adhesion condition of the metal layer to the substrate.

In the case of sequential impacts of droplets, the impact frequency influences the film stabilization by supplying kinetic and thermal energies to a system tending to stabilization. The impact of successive droplets creates air bubbles which can be expelled when the dynamics is significant enough, or trapped when the solidification is fast enough. Solidification is however much conditioned by the impact of the first series and less influenced by the next layers. Thus, gas traps, blocked by the metal solidification during the impact and the spreading of the firsts layers, are difficult to eliminate by following impacts, despite the possible remelting of the metal.

As a perspective, simulations will be extended to investigate the influence of the impact frequency on the coating and the distance D_g between two neighbouring droplets.

References

[1] Z. Zhao, D. Poulikakos, Heat transfer and fluid dynamics during the collision of a liquid droplet on a substrate—II. Experiments., Internat. J. Heat Mass Transfer 39 (13) (1996) 2791–2802.

[2] M. Fukumoto, E. Nishioka, T. Matsubara, Flattening and solidification behavior of a metal droplet on a flat substrate surface held at various temperatures, Surface Coatings Technol. 120–121 (1999) 131–137.

[3] M. Vardelle, A. Vardelle, A.C. Léger, P. Fauchais, D. Gobin, Influence of particle parameters at impact on splat formation and solidification in plasma spraying processes, J. Thermal Spray Technol. 4 (1) (1994) 50–58.

[4] S. Schiaffino, A.A. Sonin, Molten droplet deposition and solidification at low Weber numbers, Phys. Fluids 9 (11) (1997) 3172–3187.

[5] Q. Xu, E.J. Lavernia, Influence of nucleation and growth phenomena on microstructural evolution during droplet-based deposition, Acta Mater. 49 (2001) 3849–3861.

[6] M. Pasandideh-Fard, S. Chandra, J. Mostaghimi, A three-dimensional model of droplet impact and solidification, Internat. J. Heat Mass Transfer 45 (11) (2002) 2229–2242.

[7] C. Robert, A. Vardelle, D. Gobin, P. Fauchais, Modeling of rapid solidification in plasma spray deposition, High Temp. Material Processes (1998) 225–244.

[8] J. Madejski, Solidification of droplets on a cold surface, Internat. J. Heat Mass Transfer 19 (1976) 1009–1013.

[9] S. Sampath, X.Y. Jiang, J. Matejicek, A.C. Léger, A. Vardelle, Substrate temperature effects on splat formation, microstructure development and properties of plasma sprayed coatings Part I: Case study for partially stabilized zirconia, Materials Sci. Engrg. A 272 (1999) 181–188.

[10] S. Harfel, D. Poulikakos, Experimental investigation of the transient impact fluid dynamics and solidification of a molten microdroplet pile-up, Internat. J. Heat and Mass Transfer 46 (2003) 535–550.

[11] E. Arquis, J.P. Caltagirone, Sur les conditions hydrodynamiques au voisinage d'une interface milieu fluide-milieu poreux: Application à la convection naturelle, C. R. Acad. Sci. Sér IIb 299 (1984) 1–4.

[12] S.V. Patankar, Numerical Heat Transfer and Fluid Flow, Hemisphere, New York, 1980.

[13] M. Fortin, R. Glowinski, Méthode de Lagrangien Augmenté. Application à la Résolution Numérique des Problèmes aux Limites, Collection Méthodes Mathématiques de l'Informatique, Dunod, Paris, 1982.

[14] S. Vincent, J.-P. Caltagirone, A one-cell local multigrid method for solving unsteady incompressible multiphase flows, J. Comput. Phys. 163 (2000) 172–215.

[15] J.U. Brackbill, D.B. Kothe, C. Zemach, A continuum method for modeling surface tension, J. Comput. Phys. 100 (1992) 335–354.

[16] S. Vincent, J.-P. Caltagirone, Efficient solving method for unsteady incompressible interfacial flow problems, Internat. J. Numer. Methods fluids 30 (1999) 795–811.

[17] D.L. Youngs, Time-dependent multimaterial flow with large fluid distortion, in: K.W. Morton, M.J. Baines (Eds.), Numer. Methods Fluid Dynamics, Academic Press, New York, 1982.

[18] D. Jamet, O. Lebaigue, N. Coutris, J.M. Delhaye, The second gradient method for the direct numerical simulation of liquid vapor flows with phase change, J. Comput. Phys. 169 (2) (2001) 624–651.

[19] V.R. Voller, Fast implicit finite-difference method fo rthe analysis of phase change problems, Numer. Heat Transfer 17 (B) (1990) 155–169.

[20] S. Vincent, E. Arquis, Numerical modelling of cooling and solidification of molten particles impacting a solid substrate, High Temp. Material Processing 4 (1) (2000) 79–102.

[21] S. Vincent, J.P. Caltagirone, E. Arquis, Refroidissement et solidification de gouttelettes impactant sur un substrat solide, Société Française de Thermique 7 (1999) 443–448.

[22] H.-Y. Kim, J.-H. Chun, The recoiling of liquid droplets upon collision with solid surfaces, Phys. Fluids 13 (3) (2001) 643–659.

[23] M. Francois, W. Shyy, Computations of drop dynamics with the immersed boundary method; Part 1—Numerical algorithm and buoyancy induced effect, Numer. Heat Transfer B 44 (2003) 101–118.

[24] M. Francois, W. Shyy, Computations of drop dynamics with the immersed boundary method; Part 2—Drop impact and heat transfer, Numer. Heat Transfer B 44 (2003) 119–143.
[25] D. Attinger, Z. Zhao, D. Poulikakos, An experimental study of molten microdroplet surface deposition and solidification: transient behavior and wetting angle dynamics, ASME J. Heat Transfer 122 (2000) 544–556.
[26] C. Le Bot, E. Arquis, Direct numerical simulation of the manufacturing of a coating on a substrate by projection, in: Proceedings of ASME FEDSM '02, ASME 2002 Fluids Engineering, Division Summer Meeting, Montreal, Quebec, Canada, 2002, pp. 1–6.
[27] S. Vincent, J.-P. Caltagirone, E. Arquis, Direct numerical simulation of liquid droplet flattening on both solid substrate and liquid film, in: Second International Symposium on Two-Phase Flow Modelling and Experimentation, vol. 2, Pise, Italy, 1999, pp. 995–1002.
[28] T. Loulou, D. Delaunay, Technical notes: The interface temperature of two suddenly contacting bodies, one of them undergoing phase change, Internat. J. Heat Mass Transfer 40 (7) (1997) 1713–1716.
[29] S. Harfel, D. Poulikakos, Transport and solidification phenomena in molten microdroplet pileup, J. Appl. Phys. 92 (3) (2002) 1675–1689.